Influence of Bias-Enhanced Nucleation on Thermal Conductance Through Chemical Vapor Deposited Diamond Films

Baratunde A. Cola, Ratnakar Karru, Changrui Cheng, Xianfan Xu, and Timothy S. Fisher

***Abstract*—This work describes an experimental study of the cross-plane thermal conductance of plasma-enhanced chemical vapor deposited (PECVD) diamond films grown as a result of bias-enhanced nucleation (BEN). The diamond films are grown on silicon wafers using a two-step process in which a nucleation layer of amorphous or diamond like (DLC) carbon is first deposited on the silicon under the influence of a voltage bias. Then, conditions are adjusted to allow for polycrystalline diamond (PD) growth. The nucleation layer is essential for seeding diamond growth on smooth substrates and for optimizing PD properties such as grain size, orientation, transparency, adhesion, and roughness. A photoacoustic (PA) technique is employed to measure the thermal conductivities of and the thermal interface resistances between the layers in the diamond film structure. The influence of nucleation layers that are 70, 240, 400, and 650 nm thick on the thermal conductance of the diamond film structure is characterized. The thermal conductivity of the nucleation layer exhibits a thickness dependence for relatively thin layers. For each sample, the thermal conductivity of the PD is higher than 500 W·m^{-1}K^{-1} (measurement sensitivity limit). A resistive network for the diamond film structure is developed. The resistance at the silicon/nucleation interface is less than 10^{-9}m^2·K·W^{-1} (measurement sensitivity limit), which is of the order of theoretical predictions. The minimum diamond film structure resistance occurs when the nucleation layer is thinnest. When the nucleation layer is sufficiently thick, it begins to exhibit bulk behavior, and the resistance at the nucleation/PD interface dominates the thermal resistance of the diamond film structure.**

***Index Terms*—Coatings, diamond, microelectronics, photoacoustic, plasma-enhanced chemical vapor deposited (PECVD), thermal interface resistance, thin films.**

NOMENCLATURE

a	$\sqrt{\pi f/\alpha}$, m^{-1}.
B	Intermediate coefficient.
f	Modulation frequency, s^{-1}.
I	Intensity of laser light, W·m^{-2}.
j	Imaginary unity.
k	Thermal conductivity, W·m^{-1}K^{-1}.
Δk	Thermal conductivity uncertainty, W·m^{-1}K^{-1}.
l	Thickness, m.
R	Thermal interface resistance, m$^2 \cdot$ K $\cdot$ W^{-1}.
ΔR	Thermal interface resistance uncertainty, m^2·K·W^{-1}.
t	Time, s.

Greek symbols

α	Thermal diffusivity, m^2·s^{-1}.
ϕ	Phase shift.
θ	Complex temperature, K.
ρ	Reflectivity.
σ	$(1+j)a$, m^{-1}.
ω	Modulated angular frequency, 2·π·s^{-1}.

Subscripts

n	Nucleation layer.
n/PD	Nucleation and polycrystalline diamond interface.
PD	Polycrystalline diamond layer.
s/n	Silicon and nucleation interface.
T	Diamond film structure.

Manuscript received November 22, 2006; revised April 27, 2007. This work was supported by the NASA Institute for Nanoelectronics and Computing (INaC) and Purdue University. This work was recommended for publication by Associate Editor B. Sammakia upon evaluation of the reviewers comments.

B. A. Cola, R. Karru, X. Xu, and T. S. Fisher are with Purdue University, West Lafayette, IN 47907 USA (e-mail: tsfisher@purdue.edu).

C. Cheng is with Butler International, Inc., West Lafayette, IN 47907 USA.

Color versions of one or more of the figures in this paper are available online at http://ieeexplore.ieee.org.

Digital Object Identifier 10.1109/TCAPT.2007.906725

I. INTRODUCTION

BECAUSE of the steady increase in device density of electronic circuits and components, driven by improvements in fabrication technologies, effective and efficient thermal management is required to alleviate problems that lead to poor reliability and longevity. Because of its extreme hardness, mechanical stability, chemical inertness, dielectric strength, and high thermal conductivity, diamond can be an excellent packaging material [1]–[7]. The thermal conductance of diamond films has been measured in several studies [8]–[13]. The high in-plane and cross-plane thermal conductivities of diamond make it particularly effective to spread heat away from hot spots to a heat sink. However, as heat dissipation increases, the thermal resistance of the nucleation layer and its associated interfaces will consume a larger portion of the thermal budget. Despite its obvious advantages as a thermal enhancement material, polycrystalline diamond films have not been widely used in microelectronic components, largely because of difficulties in

1521-3331/$25.00 © 2007 IEEE

heterogeneous material integration and cost. Here, we consider the thermal characteristics of a promising material integration approach involving bias-enhanced nucleation (BEN) [14] of plasma-enhanced chemical vapor deposited (PECVD) diamond films.

To ensure the suitability of diamond films in a cooling design, thermal conductance must be measured, preferably by a nonintrusive technique, and the effect of nucleation on thermal performance should be characterized. In this work, a photoacoustic (PA) technique [15]–[17] is used to measure the thermal conductivities of and the thermal interface resistances between nucleation and polycrystalline diamond (PD) layers. The thermal conductivities are used in conjunction with measured thicknesses to calculate the thermal resistance of each layer; these resistances are summed in series with the interface resistances to determine the thermal resistance of the diamond film structure.

PECVD has become a popular method to synthesize diamond films for microelectronic applications because it offers low sample contamination, relatively low growth temperatures, and an ability to control the film characteristics [18]. During the synthesis of such films using PECVD and BEN, the formation of an amorphous carbon or diamond like carbon (DLC) layer (nucleation stage) precedes the growth of well faceted diamond grains (growth stage) [7], [19]. In this study, we examine the thermal behavior of the products of each stage of the growth process separately as well as together, with attention given to the nucleation conditions and time allowed for nucleation. By examining thermal conductance in this piecewise manner, we seek to elucidate the factors that contribute to a PECVD synthesized diamond film's overall thermal resistance, thereby allowing more thorough understanding of its thermal performance.

II. Experimental Methods

A. Film Synthesis and Sample Preparation

The films used in this study were synthesized in a SEKI AX5200S microwave plasma CVD system. A molybdenum holder concentrates the plasma over silicon substrates (0.580 mm thick). Substrate pretreatment, such as ultrasonic scratching with diamond powder, is usually required to deposit diamond films on silicon surfaces [19]. However, such a treatment is undesirable in applications where surface roughness needs to be small. BEN is a well established alternative to attain high nucleation densities on smooth surfaces such as silicon [19]–[23]. BEN eliminates the need for additional cleaning steps because it occurs in the deposition chamber under the same vacuum environment used for diamond film growth. For this study, a constant DC bias of -250 V was applied during the nucleation stage [14]. This bias level was found to produce successful nucleation on silicon in our system [7].

Methane and hydrogen were used as the source gases, and nucleation was carried out in 300 W plasma for 15, 30, 45, and 60 min. While diamond film synthesis usually occurs at much higher plasma powers (more than 1 kW), 300 W was used for nucleation in this study because plasma arching was observed at both high plasma power and high bias voltage. After nucleation, the bias was turned off for the growth stage to allow the plasma power to increase. 1200 W plasma power was used during the growth stage to promote the growth of thick films. A chamber pressure above 55 torr is required to safely support a plasma power above 1000 W in our system. The process parameters are summarized in Table I, and a typical film structure is shown in Fig. 1. For each nucleation duration, two different samples were fabricated: a sample consisting of a silicon substrate and a nucleation layer (herein referred to as the "nucleation sample"), and a sample consisting of a silicon substrate, a nucleation layer, and a PD film (herein referred to as the "PD growth sample"). Typical Raman spectra of the nucleation and PD growth samples are shown in Fig. 2. The low signal to noise ratio and the presence of a G-band mode in the PD growth samples' spectra are due to the simultaneous excitation of the PD and nucleation layers. The Raman spectra supports field-emission scanning electron microscope (FESEM) observations of an amorphous-like carbon film in the nucleation layer and diamond growth in the PD layer. As determined from FESEM, the average particle size in the nucleation layers ranged from 5 to 25 nm; the average increased with increased nucleation time. Consequently, the average surface roughness of the nucleation layer increased with nucleation time as well. The average PD grain size ranged from 1 to 3 μm and slightly increased as the nucleation time increased.

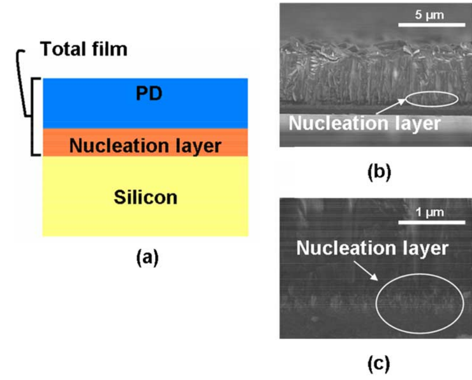

Fig. 1. (a) Schematic of a typical diamond film grown by PECVD using BEN. The silicon wafer is 580 μm thick. (b) FESEM of diamond film for 45-min nucleation time. (c) Higher resolution (6.5 X) FESEM that shows a close up of the nucleation layer.

B. Photoacoustic (PA) Technique

The PA technique is one of many proven techniques to measure thermal conductivity of thin films, and it has recently been used to measure the thermal resistance of separable interfaces [17]. The PA technique provides high accuracy [16], yet in comparison to other techniques to measure thermal conductance across thin films and planar interfaces, it is relatively simple to implement. Reference [15] provides a detailed description of the technique.

Theory: The sample used for PA measurement can have a backing layer (0) and N successive layers (1, 2,$\ldots,N$) on which the x-coordinate originates from the surface of layer N and points outward. The multilayered material is heated by a modulated laser beam with an intensity of $1/2 \cdot I_o(1+\cos(\omega t))$, and absorption of the laser beam is allowed in any layer, and in more than one layer. The backing material (0) and a gas medium $(N+1)$ in contact with the surface layer (N) are considered to be thermally thick. The transient temperature field in the multilayer sample and gas can be derived by solving

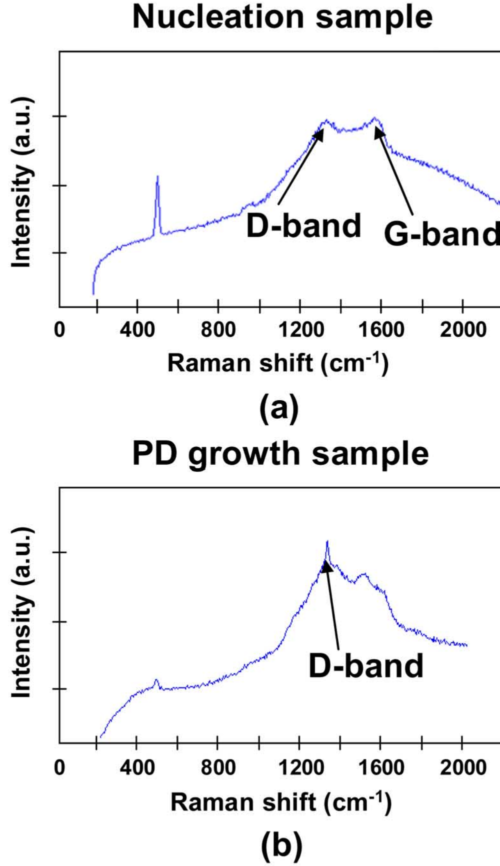

Fig. 2. (a) Raman spectrum for the nucleation layer. The merging of the D-band and G-band suggests the presence of an amorphous carbon state. (b) Raman spectrum for the PD layer. The D-band peak near 1320 cm^{-}1 can indicate a preference for diamond. The peak near 500 cm^{-}1 is from silicon.

TABLE I
PROCESS PARAMETERS FOR THE GROWTH OF PECVD DIAMOND FILMS

Parameter	Nucleation	PD growth
Gas flow rate (sccm) H_2: CH_4	200:10	200:2
Plasma power (W)	300	1200
Bias (V)	250	0
Pressure (torr)	15	60
Duration (hr)	0.25, 0.5, 0.75, 1	10

a set of 1-D heat conduction equations [15], [24]. Details of the derivation process have been described in [15]. The solution of the complex temperature distribution θ_{N+1} in the gas can be expressed as

$$\theta_{N+1} = (1-\rho) \cdot B_{N+1} e^{-\sigma_{N+1} x} e^{j\omega t} \quad (1)$$

where B_{N+1} is complex, and is a function of the thermal properties of the multilayered sample. The general formulation of B_{N+1} is long and readily available in the literature; thus the reader is referred to [15]–[17] for its full formulation.

The temperature in the gas layer is related to the phase shift and the amplitude of the pressure or PA signal using a thermal piston analogy where the heated gas near the sample surface pushes the rest of the gas up like a piston [15]. The phase shift of the PA signal is calculated as $\mathrm{Arg}(B_{N+1}) - \pi/4$, and the amplitude of the PA signal is calculated as $\mathrm{Abs}[(1-\rho) \cdot B_{N+1} P_o / \sqrt{2} l_{N+1} a_{N+1} T_o]$, where T_o and P_o are the ambient temperature and pressure, respectively.

Experimental Details: The experimental setup is shown schematically in Fig. 3. A fiber laser is used as the heating source. An acoustic-optical modulator (AOM) driven by a function generator modulates the laser power with a sinusoidal function. For this study, the modulation frequency ranges from 2 to 20 kHz, and the output power of the laser is approximately 350 mW at the modulation mode. The laser beam is reflected and focused and then directed onto the sample mounted at the bottom of the PA cell. To promote complete laser power absorption at the sample surface, 80 nm of titanium is deposited on the samples. The PA cell is the same as the one used in the studies of [17]. The acoustic signal is sensed by a microphone embedded in the side wall of the cell. The signal is transferred to the lock-in amplifier, where the amplitude and phase are measured. The phase shift of the acoustic signal is used to determine thermal properties because it is more stable than the amplitude signal in the current experimental setup and thus provides higher measurement precision.

In order to account for delay in the PA response due to the time needed for the acoustic wave to travel from the sample surface to the microphone, and due to acoustic resonance in the cell, a silicon wafer (0.580 mm thick) is used as a reference or calibration sample. 80 nm of titanium is deposited on the silicon reference and test samples at the same time to allow for similar surface reflectivity and laser absorption. Within the frequency range of this study, the reference sample is thick enough to be considered a bulk material (much thicker than the thermal penetration depth, $1/\sqrt{\pi f/\alpha_{\mathrm{Silicon}}}$); therefore the phase shift is $-90°$. The calibrated phase shift of the sample, ϕ, is calculated as $\phi = \phi' - \phi'_{\mathrm{Silicon\ reference}} - 90$, where ϕ' is the measured phase shift for the sample, and $\phi'_{\mathrm{Silicon\ reference}}$ is the measured phase shift for the reference. The experimental setup is calibrated before each measurement and at each frequency. After the signal stabilizes, phase-shift data are recorded every 8 s and averaged every 5 min. In order to determine the drift of the signals with time, the references are also tested after each sample measurement.

The measured and calibrated phase shift of the acoustic signal is used in conjunction with the general PA model of [15] to estimate the thermal interface resistance between the silicon substrate and nucleation layer, $R_{s/n}$, and between the nucleation layer and the PD layer, $R_{n/\mathrm{PD}}$, and the thermal conductivities of the nucleation layer, k_n, and the PD layer, k_{PD}. In order to estimate theses four quantities, the nucleation samples are measured and the two unknowns, $R_{s/n}$ and k_n, are obtained. Then the PD growth samples are measured with $R_{s/n}$ and k_n input as known values, and the remaining two unknowns, $R_{n/\mathrm{PD}}$ and k_{PD}, are estimated. The sample measurement procedure is illustrated in Fig. 4. For each measurement set, the unknowns are solved by fitting the PA model to the experimental data using a least-squares algorithm where trial values of the unknown thermal properties are used to calculate the phase shift of the PA signal at each experimental frequency. The sum of the square of the difference between calculated and experimental values of phase shift is calculated. The trial R and k values for which

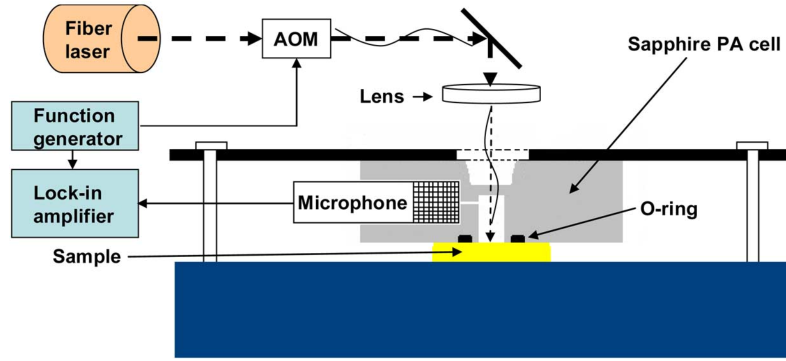

Fig. 3. Schematic diagram of the photoacoustic apparatus.

Fig. 4. In the first measurement set the nucleation sample is measured, and $R_{s/n}$ and k_n are determined. These measured values are then used in the second measurement set (PD growth sample) to determine $R_{n/\mathrm{PD}}$ and k_{PD}. The sample layer labeling used in the PA model is presented for each measurement set as well.

the least square is obtained are taken as the property values. The piecewise examination of the diamond film structures allows for each measurement set to have only two unknowns (R and k) that are uncoupled in the governing equations, thereby allowing the least-squares fits to be unique.

Experimental uncertainty is primarily determined by the uncertainty in thickness measurements, and for the PD growth samples, the uncertainty in the k_n and $R_{s/n}$ measurements as well. The effects of uncertainties associated with other 'known' material properties used in the PA model, uncertainty associated with laser energy drift, and uncertainty associated with phase shift measurements were negligible in comparison. Uncertainty in the measured thermal properties is determined by finding the range of the property values that result from changing the nucleation and PD layer thicknesses, and (for the PD growth samples) k_n and $R_{s/n}$ within their uncertainty range in the PA model.

The PA signal is primarily influenced by the sample layers or interfaces that are the most resistive to heat flow. Consequently, there are limits on the magnitudes of property values that can be sensed with the technique. These limitations are determined by experimental error and/or by varying the desired property in the PA model to conditions where further changes in the property

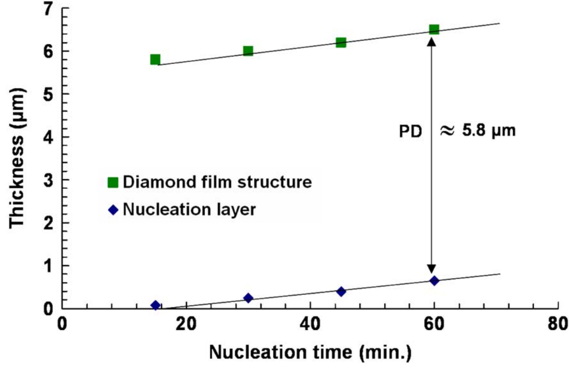

Fig. 5. Thicknesses of the nucleation layer and PD as a function of nucleation time. PD growth is shown to be independent of nucleation time, and is the same thickness for each case. The measurement error, as given in Table II, is less than the size of the data point markers.

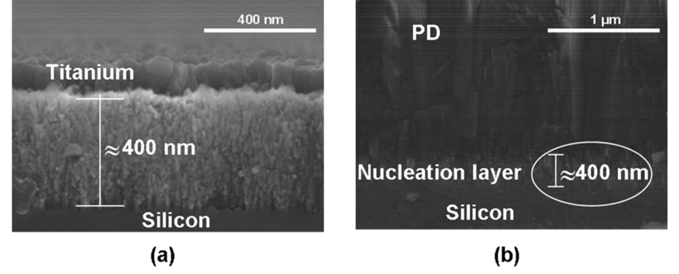

Fig. 6. FESEM of nucleation layer without (a), and with (b) PD growth for a nucleation time of 45 min. In each case, the nucleation layer is approximately 400 nm thick. The top layer in (a) is titanium, which is deposited for the purpose of laser energy absorption.

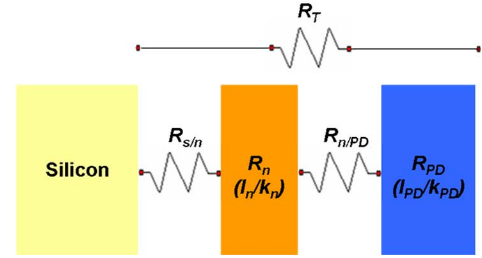

Fig. 7. Thermal circuit for diamond films synthesized by PECVD using BEN. R_T is the thermal resistance of the entire diamond film structure.

produce a negligible change in the calculated phase shift. Experimental uncertainty is sufficiently large in this study that the sensitivity limits are determined by it alone. If the thermal conductivity uncertainty for a layer is Δk, then the smallest measurable thermal interface resistance for that layer is approximately $l \cdot \Delta k / k^2$. Similarly, if the uncertainty of the interface resistance is ΔR, then the largest measurable thermal conductivity for that layer is approximately $1/\Delta R$.

III. Results and Discussion

The thermal resistances of PECVD-via-BEN diamond films were measured on samples with nucleation times of 15, 30, 45, and 60 min. First, only nucleation was performed, and the layer formed in each case was analyzed. Then, on new samples, nucleation followed by 10 h of PD growth forms the diamond film structure. The thicknesses of the nucleation layer and the diamond film structure were measured from FESEM images, and the resulting data are presented in Table II. The PD layer thickness is determined by identifying the boundary between nucleation and PD in the diamond film structure FESEM image. For each case, the location of this boundary coincided with the measured thickness of the nucleation layer (without PD), thus corroborating this result. The amount of PD grown is approximately the same for each nucleation time, as shown in Fig. 5. Fig. 6 shows that the nucleation layer retains its pre-PD growth thickness after the PD is grown, verifying an important assumption in our analysis. A thermal resistance network for the diamond film structure is presented in Fig. 7. The thermal resistance of the nucleation and PD layers are given as $R_n = l_n/k_n$ and $R_{\mathrm{PD}} = l_{\mathrm{PD}}/k_{\mathrm{PD}}$, respectively.

A summary of resistances for the diamond film structure is shown in Table III, and the data trend is illustrated in Fig. 8. As discussed in detail later, the large jump in resistance from a nucleation layer thickness of 400 to 650 nm is due to poor bonding of the PD to the 650 nm-thick nucleation layer. $R_{s/n}$ is the first resistance encountered by heat flowing from silicon to a diamond film as shown in Fig. 7. This resistance is the result of acoustic mismatch and imperfect interfacial contact, and theoretical modeling by Zeng and Chen suggest that it is very small, on the order of $10^{-9}\mathrm{m}^2\cdot\mathrm{K}\cdot\mathrm{W}^{-1}$ [25]. For the samples in this study, $R_{s/n}$ is less than the smallest resistance that can be sensed

TABLE II
Thickness as a Function of Nucleation Time for the Nucleation Layer and Diamond Film Structure. Uncertainty in the Thickness Measurements is Estimated From the Precision of the Scale Bars in FESEM Images

Nucleation time (min.)	Nucleation thickness (µm)	Diamond film structure thickness* (µm)
15	0.07 ± 0.01	5.80 ± 0.02
30	0.24 ± 0.02	6.00 ± 0.02
45	0.40 ± 0.02	6.20 ± 0.02
60	0.65 ± 0.02	6.50 ± 0.02

* 10 hour growth after nucleation

with our experimental technique. These sensitivity minima are all on the order of $10^{-9}\mathrm{m}^2\cdot\mathrm{K}\cdot\mathrm{W}^{-1}$; therefore, we conclude that the nucleation layer is in good contact with the silicon substrate, and $R_{s/n}$ is predicted relatively well by the modeling of Zeng and Chen. The next resistive path in the diamond film network is R_n. Each R_n value is calculated from the k_n measurements for the different nucleation samples. A thickness dependence of the nucleation layer's thermal conductivity is apparent for relatively thin layers, causing a nonlinear relationship between l_n and R_n as illustrated in Fig. 8. As the layer becomes sufficiently thick, k_n converges to a consistent value, and R_n begins to display a linear relationship with respect to l_n as expected. This trend can be explained by the change in the structure of the nucleation layer with increased thickness. The nucleation layer is more discontinuous and has smaller particle sizes (e.g., more grain boundaries and voids) near its interface with the silicon substrate than in the section of the layer that accumulates with increasing thickness. Thus, as the nucleation layer becomes

TABLE III
RESISTANCE COMPONENTS OF DIAMOND FILMS SYNTHESIZED BY PECVD USING BEN. UNCERTAINTY IN THE RESISTANCE VALUES IS THE RESULT OF UNCERTAINTY IN THE THICKNESS AND k_n MEASUREMENTS. $R_{s/n}$ AND R_{PD} ARE BELOW THE MEASUREMENT SENSITIVITY

	Nucleation		PD		Diamond film structure
Nucleation time (min.)	$R_{s/n}$ (10^{-7} m^2 K W^{-1})	R_n (10^{-7} m^2 K W^{-1})	$R_{n/PD}$ (10^{-7} m^2 K W^{-1})	R_{PD} (10^{-7} m^2 K W^{-1})	R_T (10^{-7} m^2 K W^{-1})
15	< 0.04	0.17 ± 0.04	0.63 ± 0.06	< 0.12	~ 0.9
30	< 0.05	0.45 ± 0.05	0.98 ± 0.09	< 0.12	~ 1.5
45	< 0.05	0.48 ± 0.05	1.11 ± 0.11	< 0.12	~ 1.7
60	< 0.06	0.74 ± 0.06	5.18 ± 0.12	< 0.12	~ 6.0

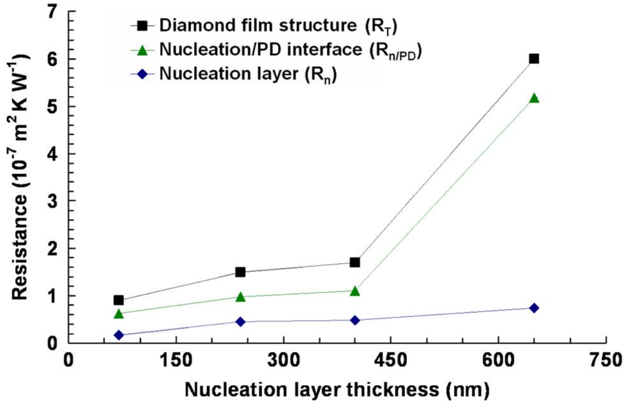

Fig. 8. Dominate resistance components, R_n and $R_{n/PD}$, of the diamond films' thermal resistance, R_T, as a function of nucleation layer thickness. The measurement error, as given in Table III, is less than the size of the data point markers.

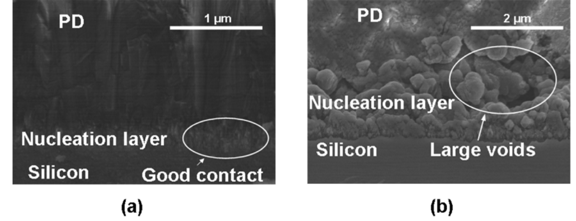

Fig. 9. (a) Nucleation/PD interface after 45 min of nucleation. The nucleation layer and the PD layer appear well connected. (b) Nucleation/PD interface after 60 min of nucleation. Stress-induced voids are present at the nucleation/PD interface.

thicker, the more continuous section with larger particles (away from the interface) grows thicker and has a greater influence on the measured k_n, and eventually dominates thermal transport across this layer. The measured k_n values are larger than the room-temperature thermal conductivity value of amorphous carbon, 1.60 $\mathrm{W{\cdot}m^{-1}K^{-1}}$ [26]; therefore, it is reasonable to assume that the carbon in the nucleation layer is DLC, which contains higher crystal order than amorphous carbon.

As presented in Table III and illustrated in Fig. 8, $R_{n/\mathrm{PD}}$ most significantly affects the thermal performance of the diamond film structure. $R_{n/\mathrm{PD}}$ decreases with decreasing nucleation layer thickness because of reduced growth or thermal stresses at the nucleation/PD interface. We postulate that when the nucleation layer becomes sufficiently thick, the thermal stresses generated at its interface with the PD weakens the bond between the nucleation layer and the PD and may cause the section of the nucleation layer near the PD interface to break into clusters, creating voids. This adverse effect may be exacerbated by the fact that the surface roughness of the nucleation layer increases as the nucleation layer thickens. This weakening of the nucleation/PD interfacial bond impedes thermal transport across the interface. To further demonstrate this point, the PD growth samples were cut in half after testing and their cross-sections were imaged with a field-emission scanning electron microscope. As illustrated in Fig. 9, the thickest nucleation layer (60 min nucleation time) resulted in the formation of large voids in the nucleation/PD interface; such voids will impede thermal transport across the interface. Additionally, for 60 min of nucleation, the PD layer's adhesion was very poor as evidenced by easy peeling of the diamond layer from the substrate (due most likely to increased stress concentration at the discrete contact points).

R_{PD} is the final resistive component of the diamond film structure. Each R_{PD} value is determined from the measured k_{PD} for the different PD growth samples. For each sample, k_{PD} is measured to be above the largest thermal conductivity that can be sensed with our experimental technique (approximately 500 $\mathrm{W{\cdot}m^{-1}K^{-1}}$). Because each PD layer is approximately 5.8 μm thick and has an average grain size between 1 and 3 μm, k_{PD} is expected to be near $10^3\mathrm{W{\cdot}m^{-1}K^{-1}}$ [8], which is consistent with the results of this study. For each sample (since l_{PD} is constant for each nucleation layer sample), R_{PD} is below approximately $10^{-8}\mathrm{m^2{\cdot}K{\cdot}W^{-1}}$ and has a negligible effect on the overall thermal resistance of the diamond film structure, R_T.

The minimum conduction resistance of the diamond film structure occurs when the nucleation layer is thinnest because of reduced thermal stress between the nucleation and PD layer. We also note that the quality, hence thermal conductivity, of PD is expected to increase with increasing nucleation layer thickness or "seeding grain" size (the nucleation layer surface asperities may be view as the seeding grains) due to the formation of larger, more continuous PD columns that promote a decrease in phonon-grain boundary scattering [1], [8]. However, as shown in this work, increased PD thermal conductivity, via increased nucleation layer thickness, would be entirely offset by increases in both R_n and $R_{n/\mathrm{PD}}$ to produce a larger overall thermal resistance (R_T).

IV. CONCLUSION

The thermal resistances of PECVD diamond films grown from BEN layers have been measured for nucleation times of 15, 30, 45, and 60 min. An experimental technique, using PA

measurements, has been employed to measure the resistive components of the diamond film structure. The resistance at the silicon/nucleation boundary and the intrinsic resistance of the PD layer were measured to have a negligible effect on the diamond film structures' resistance. For each nucleation sample, the dominant resistances in the thermal network are the intrinsic resistance of the nucleation layer and the nucleation/PD interface resistance.

In general, this study shows that the thermal resistance of PECVD diamond films grown from BEN strongly depends on the structure of the nucleation layer and the quality of the nucleation/PD interface. The thermal conductivity of the nucleation layer is measured to be higher than that of amorphous carbon and exhibits a thickness dependence for relatively thin layers, while it converges to a consistent value when the layer is sufficiently thick. Under the conditions of this study, smaller nucleation times and consequentially thinner nucleation layer thicknesses result in lower diamond film structure resistances. As the nucleation layer thickens, the nucleation/PD interface resistance, which dominates the overall resistance of the diamond film, increases because of poor interfacial bonding.

In this study, the voltage bias, plasma conditions, and gas flow ratios are the same for each case. Further work is recommended to investigate the effects of these parameters on the structure of the nucleation layer and its boundaries. The only substrate used in this study is silicon. Diamond films grown by PECVD using BEN on other relevant substrates remain to be explored. Finally, the PD layers grown in this study are all approximately 5.8 μm thick, the effect of PD layers of different thicknesses on the nucleation/PD interface resistance is suggested for further study.

Acknowledgment

The authors wish thank A. Franklin, Dr. M. R. Maschmann, and Dr. P. B. Amama for their help with FESEM and Raman characterization.

References

[1] K. E. Goodson and Y. S. Ju, "Heat conduction in novel electronic films," *Annu. Rev. Mater. Sci.*, vol. 29, pp. 261–293, 1999.
[2] R. F. Davis, *Diamond Films and Coatings*. Norwich, NY: William Andrew Publishing, 1993.
[3] M. N. R. Ashfold, P. W. May, C. A. Rego, and N. M. Everitt, "Thin film diamond by chemical vapour deposition methods," *Chem. Soc. Rev.*, vol. 23, pp. 21–31, 1994.
[4] K. E. Spear and J. P. Dismukes, *Synthetic Diamond: Emerging CVD Science and Technology*. Hoboken, NJ: Wiley, 1994.
[5] X. Zhu, D. M. Aslam, Y. Tang, B. H. Stark, and K. Najafi, "The fabrication of all-diamond packaging panels with built-in interconnects for wireless integrated microsystems," *J. Microelectromech. Syst.*, vol. 13, no. 3, pp. 396–405, 2004.
[6] X. Zhu and D. M. Aslam, "CVD diamond thin film technology for MEMs packaging," *Diamond Rel. Mater.*, vol. 15, no. 2–3, pp. 254–258, 2006.
[7] J. Chee, R. Karru, T. S. Fisher, and D. Peroulis, "DC-65 GHz characterization of nanocrystalline diamond leaky film for reliable RF MEMS switches," in *Proc. Eur. Microw. Conf.*, 2005, vol. 3, pp. 1527–1530.
[8] J. E. Graebner, S. Jin, G. W. Kammlott, J. A. Herb, and C. F. Gardinier, "Large anisotropic thermal conductivity in synthetic diamond films," *Nature*, vol. 359, pp. 401–, 1992.
[9] K. E. Goodson, O. W. Käding, M. Rösler, and R. Zachai, "Experimental investigation of thermal conduction normal to diamond-silicon boundaries," *J. Appl. Phys.*, vol. 77, no. 4, pp. 1385–1392, 1995.
[10] J. E. Graebner, "Measurements of thermal conductivity and thermal diffusivity of CVD diamond," *Int. J. Thermophys.*, vol. 19, no. 2, pp. 511–523, 1998.
[11] H. Verhoeven, H. Reiß, H.-J. Füßer, and R. Zachai, "Thermal resistance of thin diamond films deposited at low temperatures," *Appl. Phys. Lett.*, vol. 69, no. 11, pp. 1562–1564, 1996.
[12] J. Hartmann, P. Voigt, and M. Reichling, "Measuring local thermal conductivity in polycrystalline diamond with a high resolution photothermal microscope," *J. Appl. Phys.*, vol. 81, no. 7, pp. 2966–2972, 1997.
[13] E. Jansen and E. Obermeier, "Thermal conductivity measurements of thin films based on micromechanical devices," *J. Micromech. Microeng.*, vol. 6, pp. 118–121, 1996.
[14] J. Robertson, J. Gerber, S. Sattel, M. Weiler, K. Jung, and H. Ehrhardt, "Mechanism of bias-enhanced nucleation on Si," *Appl. Phys. Lett.*, vol. 66, no. 24, pp. 3287–3289, 1995.
[15] H. Hu, X. Wang, and X. Xu, "Generalized theory of the photoacoustic effect in a multilayer material," *J. Appl. Phys.*, vol. 86, no. 7, pp. 3953–3958, 1999.
[16] X. Wang, H. Hu, and X. Xu, "Photoacoustic measurement of thermal conductivity of thin films and bulk materials," *ASME J. Heat Transf.*, vol. 123, pp. 138–144, 2001.
[17] B. A. Cola, J. Xu, C. Cheng, H. Hu, X. Xu, and T. S. Fisher, "Photoacoustic characterization of carbon nanotube array interfaces," *J. Appl. Phys.*, vol. 101, no. 054313, 2007.
[18] E. Kohn, M. Adamschik, P. Schmid, A. Denisenko, A. Aleksov, and W. Ebert, "Prospects of diamond devices," *J. Phys. D: Appl. Phys.*, vol. 34, pp. R77–R85, 2001.
[19] S.-T. Lee, Z. Lin, and X. Jiang, "CVD diamond films: Nucleation and growth," *Mater. Sci. Eng.*, vol. 25, pp. 123–154, 1999.
[20] B. R. Stoner, G.-H. M. Ma, S. D. Wolter, and J. T. Glass, "Characterization of bias-enhanced nucleation of diamond on silicon by *in vacuo* surface analysis and transmission electron microscopy," *Phys. Rev. B*, vol. 45, no. 19, pp. 11067–11084, 1992.
[21] M. Schreck, K.-H. Thürer, and B. Stritzker, "Limitations of the process window for the bias-enhanced nucleation of heteroepitaxial diamond films on silicon in the time domain," *J. Appl. Phys.*, vol. 81, no. 7, pp. 3092–3095, 1997.
[22] S. D. Wolter, F. Okuzumi, J. T. Prater, and Z. Sitar, "AC vs. DC bias-enhanced nucleation of highly oriented diamond on silicon (100)," *J. Electrochem. Soc.*, vol. 149, no. 2, pp. G114–G117, 2002.
[23] A. N. Jones, W. Ahmed, C. A. Rego, M. J. Jackson, and R. Hall, "Nucleation studies of pulsed bias-enhanced CVD of diamond on biomaterials," *J. Mater. Eng. Perform.*, vol. 15, no. 2, pp. 192–194, 2006.
[24] R. S. Quimby and W. M. Yen, "On the adequacy of one-dimensional treatments of the photoacoustic effect," *J. Appl. Phys.*, vol. 51, no. 2, pp. 1252–1253, 1980.
[25] T. Zeng and G. Chen, "Phonon heat conduction in thin films: Impact of thermal boundary resistance and internal heat generation," *ASME J. Heat Transf.*, vol. 123, pp. 340–347, 2001.
[26] F. P. Incropera and D. P. DeWitt, *Heat and Mass Transfer*, 5th ed. Hoboken, NJ: Wiley, 2002.

Baratunde A. Cola received the B.E. and M.S. degrees in mechanical engineering from Vanderbilt University, Nashville, TN, in 2002 and 2004, respectively, and is currently pursuing the Ph.D. degree in mechanical engineering at Purdue University, West Lafayette, IN.

His current research interests include nanomaterial synthesis, applications of carbon nanotubes, and cooling of microelectronics.

Ratnakar Karru received the B.Tech. degree from the Indian Institute of Technology, Kharagpur, in 2001 and the M.S. degree in mechanical engineering from Purdue University, West Lafayette, IN, in 2003 where he is currently pursuing the M.S. degree in electrical engineering.

His research involves synthesis and characterization of diamond thin films, focusing on their applications in RF MEMS capacitive switches.

Changrui Cheng received the Ph.D. degree from the School of Mechanical Engineering, Purdue University, West Lafayette, IN, in 2006.

Currently, he works in Butler International, Inc., West Lafayette, as an Engineering Analyst. His research focuses on molecular dynamics simulation of laser micro-machining and computational modeling in thermal-fluid.

Xianfan Xu received the M.S. and Ph.D. degrees in mechanical engineering from the University of California at Berkeley in 1991 and 1994, respectively.

He is a Professor of Mechanical Engineering with Purdue University, West Lafayette, IN. His current research is laser based materials processing and diagnostics.

Timothy S. Fisher received the B.S. and Ph.D. degrees in mechanical engineering from Cornell University, Ithaca, NY, in 1991 and 1998, respectively, and the M.S. degree from Vanderbilt University, Nashville, TN, in 2002.

He joined the School of Mechanical Engineering and Birck Nanotechnology Center, Purdue University, West Lafayette, IN, in 2002 after several years at Vanderbilt University. Prior to his graduate studies, he was employed from 1991 to 1993 as a Design Engineer in Motorola's Automotive and Industrial Electronics Group. His research has included efforts in simulation and measurement of nanoscale heat transfer, coupled electro-thermal effects in semiconductor devices, nanoscale direct energy conversion, molecular electronics, microfluidic devices, hydrogen storage, and computational methods ranging from atomistic to continuum scales. His current efforts include theoretical, computational, and experimental studies focused toward integration of nanoscale materials with bulk materials for enhancement of electrical, thermal, and mass transport properties. Applications of his work cover a broad range of areas, including nanoelectronics, thermal interface materials, thermal-electrical energy conversion, biosensors, and hydrogen storage. This work has also produced related studies of controlled synthesis of nanomaterials, particularly carbon nanotubes.

Dr. Fisher is a member of Tau Beta Pi and Pi Tau Sigma. He serves on the IEEE TC-9 Committee on Thermal Phenomena in Electronics, the ASME K-6 committee on Heat Transfer in Energy Systems, ASME K-16 Committee on Thermal Management of Electronics.